Design of an Experimental Apparatus for Visualization Studies of Bubble Dynamics in Subcooled Flow Boiling at High Pressure

Junha Kang, Donggyun Seo, and Hyungdae Kim*
Department of Nuclear Engineering, Kyung Hee University,
1732 Deogyeong-daero, Yongin-Si, Gyunggi-Do, Republic of Korea
**Corresponding author: hdkims@khu.ac.kr*

1. Introduction

Subcooled boiling heat transfer occurs in many industrial applications including nuclear reactors, due to its high efficiency in heat transfer. In pressurized nuclear reactors (PWRs) such as APR1400, the heat transfer from reactor fuels and safety systems are maintained by flooding subcooled water at high pressure up to 15.5 MPa, through reactor subchannels. Recently, computational fluid dynamics (CFD) is being developed to perform accurate predictions in subcooled flow boiling. The results are to be contributed to the safety analysis of reactor subchannels and precise designs of reactor facilities.

CFD simulates the boiling phenomenon based on the wall heat flux partitioning models as shown in Table I. Kurul and Podowski [1] partitioned heat transfer between the heated wall and the liquid into three phases, single-phase convection, evaporation, and quenching. Later, Gilman and Baglietto [2] improved the preceding models by including bubble interactions. The evaporation term was divided into bubble inertia growth and microlayer evaporation, and transient conduction by bubble sliding was added. Equations (1) to (5) indicate that each term includes the dynamics of the nucleated bubbles: nucleation site density, N; bubble departure diameter, D_d; bubble departure frequency, f; microlayer thickness, δ_m. Therefore, the performance of CFD analysis on boiling heat transfer prediction is determined by accurate measurement and modeling of bubble dynamics parameters.

In this study, the limitations of bubble dynamics models used in common CFDs are analyzed based on the PWR operating conditions. An experimental apparatus that can be operated at high pressure and temperature conditions is designed based on the normal operation condition of APR1400 to obtain high-precision bubble dynamics data.

2. Bubble Dynamics Models in CFD

Bubble dynamics models including bubble departure diameter, bubble departure frequency, and nucleation site density used in common CFD are listed in Table II. The departure diameter refers to the maximum diameter of the nucleated bubbles before they depart from the corresponding site. The model developed by Kocamustafaogullari and Ishii [3] is a semi-empirical model that was validated with experimental data at various pressure of pool boiling experiments. At atmospheric pressure, the values are in the range of 2 mm. On the other hand, as the pressure increases to 13.6 MPa, the value falls into the range of 0.006 mm.

The nucleation site density model developed by Li et al. [7] considered the high-pressure system of PWRs for its use in the CFD analysis. The model is semi-empirically developed by considering the factors affecting nucleation site density. The factors include contact angle θ, pressure P, and wall superheat ΔT_{sup}. The model was validated with existing experimental data.

The bubble dynamics models commonly used in CFD are developed to be applicable under various pressure conditions. However, experimental data used to develop the prediction models were obtained in conditions under high pressures (~15.5 MPa) of pool boiling or flow boiling under intermediate pressures (~5 MPa). Therefore, high-precision measurements of bubble dynamics parameters in flow boiling are necessary for the accurate prediction of boiling heat transfer applicable to PWRs.

Table I. Wall heat flux partitioning model [1], [2]

Wall heat flux partitioning model			
q''_{wall}	Single-phase convection	$q''_{1\phi} = h_{1\phi}\left(\Delta T_{sub} + \Delta T_{sup}\right)$	(1)
	Evaporation — Inertia growth	$q''_{e,in} = \frac{4}{3}\pi\left(\frac{D_d}{4}\right)^3 \rho_v h_{fg} f N''$	(2)
	Evaporation — Microlayer evaporation	$q''_{e,ml} = \frac{2}{3}\pi\left(\frac{D_d}{4}\right)^3 \delta_m \rho_l h_{fg} f N''$	(3)
	Sliding conduction	$q''_{sc} = 2\frac{k_l(T_w - T_l)}{\sqrt{\pi\eta_l t^*}} a_{sl} t^* f N''$	(4)
	Quenching	$q''_q = \frac{2}{3}\pi\left(\frac{D_d}{4}\right)^3 \rho_h c_{ph} \Delta T_{sub} f N''$	(5)

Table II. Bubble dynamics models in CFD

Bubble parameter	Reference	Model		CFD
Bubble departure diameter	Kocamustafaogullari and Ishii [3]	$D_b = \min\left[D_{ref}\exp\left(-\frac{\Delta T_{sub}}{\Delta T_{ref}}\right), D_{max}\right]$	(6)	ANSYS Fluent
	Tolubinski and Konstanchuk [4]	$D_b = 1.5\times10^{-5}\left(\frac{\rho_l-\rho_g}{\rho_g}\right)^{0.9}\theta\sqrt{\frac{\sigma}{g(\rho_l-\rho_g)}}$	(7)	ANSYS CFX CUPID STAR-CCM+
	Unal [5]	$D_b = 2.42\times10^{-5}P^{0.709}\left(\frac{a}{b\sqrt{\varphi}}\right)$	(8)	ANSYS Fluent STAR-CCM+
Bubble departure frequency	Cole [6]	$f = \sqrt{\frac{4g(\rho_l-\rho_g)}{3D_b\rho_l}}$	(9)	ANSYS Fluent ANSYS CFX CUPID STAR-CCM+
Nucleation site density	Li et al. [7]	$N_a = N_0 f_1(\theta) f_2(P) f_3(\Delta T_{sup})$	(10)	-
	Hibiki and Ishii [8]	$N_a = \overline{N_a}\left(1-\exp\left[-\frac{\theta^2}{8\mu^2}\right]\right)\left(\exp\left[f(\rho^+)\frac{\lambda'}{R_c}\right]-1\right)$	(11)	STAR-CCM+
	Kocamustafaogullari and Ishii [9]	$N_a = f(\rho^*)r_c^{*-4.4}$	(12)	ANSYS Fluent

3. Design of High-Pressure Experimental Apparatus

3.1. Design criteria

The main goal of designing the experimental apparatus is to conduct a flow boiling heat transfer experiment under the same conditions as APR1400, including temperature (320°C), pressure (15.5 MPa), and mass flux (3500 kg/m^2·s). Therefore, four design criteria exist to modify APR1400 reactor subchannel conditions: hydraulic diameter, heating area, entrance length, and temperature, pressure, and mass flux of the working fluid.

3.1.1. Hydraulic diameter

The shape of the bubbles nucleated inside the flow channel is determined by the hydraulic diameter of the channel [10]. The shape is determined by the confinement number, Co defined as

$$\mathrm{Co} = \frac{[\sigma g(\rho_l-\rho_v)]^{0.5}}{D_h} \quad (13)$$

,where σ, g, ρ, and D_h each refer to surface tension, gravity, density, and hydraulic diameter, respectively. When Co is under 0.5, nucleated bubbles are termed isolated bubbles, while are termed confined bubbles when the number is over 0.5. Inside the subchannels of APR1400, bubbles nucleated on the fuel claddings are in form of isolated bubbles. Results in Fig. 1 show the variations of calculated Co by change of hydraulic diameter at two different pressures, 1 and 15.5 MPa. As the Co should be under 0.5 for isolated bubbles, the hydraulic diameter of the test section was determined to be 5 mm.

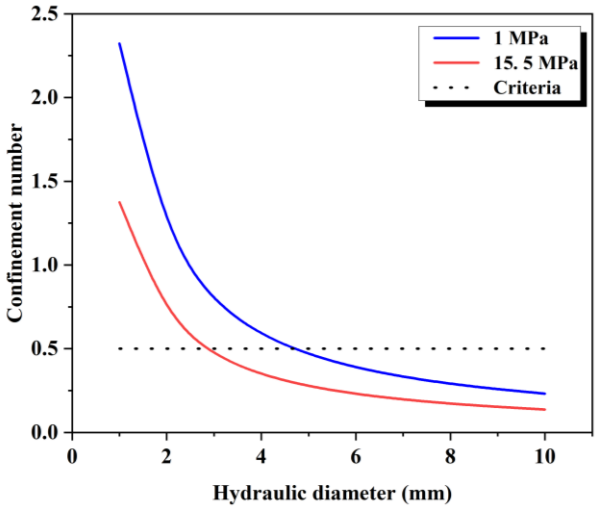

Figure 1. Confinement number variations with hydraulic diameter

3.1.2 Heating area

The heating area refers to the region where flow boiling occurs on the test sample. It is determined by predicting bubble dynamics including departure diameter, lift-off diameter, and sliding length of bubbles at experimental conditions using correlations,

$$\frac{D_d}{l_c} = 1.3(\sin\phi)^{0.4}[0.13\exp(-1.75\times10^{-4}\mathrm{Re}_l) + 0.005]\,\mathrm{Ja}_{sup}^{0.45}\exp(-0.0065\,\mathrm{Ja}_{sub}) \quad (14)$$

$$\frac{D_l}{l_c} = 1.3(\sin\phi)^{0.4}[0.20\exp(-1.28\times10^{-4}\mathrm{Re}_l) + 0.005]\,\mathrm{Ja}_{sup}^{0.45}\exp(-0.0065\,\mathrm{Ja}_{sub}) \quad (15)$$

$$l_0 = \frac{2}{3} C_v t_{sl}^{1.5} \quad (16)$$

developed by Basu et al. [11]. D_d, D_l, and l_0 each refer to departure diameter, lift-off diameter, and sliding length of bubbles, respectively. The predicted data were applied to the heating area to include every bubble dynamics.

Each parameter was calculated at the conditions of certain pressure (1 to 15.5 MPa), subcooling (20 K), and mass flux (300 to 3500 kg/m^2·s). As the result, departure and lift-off diameters had the maximum value at the conditions of 1 MPa and 300 kg/m^2·s, each having 550 μm and 800 μm as shown in Fig. 2 (a), respectively. Bubble sliding length showed the maximum value at the same condition as diameters, having 500 μm as shown in Fig. 2 (b). Therefore, considering the fact that the hydraulic diameter of the test section is 5 mm, the heating area was determined to be 4 × 8 mm^2 to cover the dynamics of all nucleated bubbles on the heating surface.

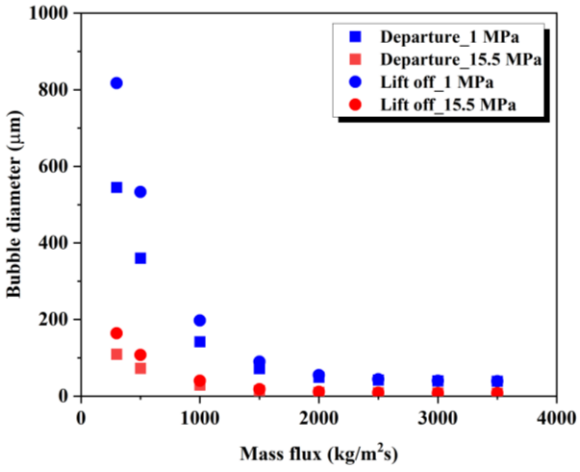

(a)

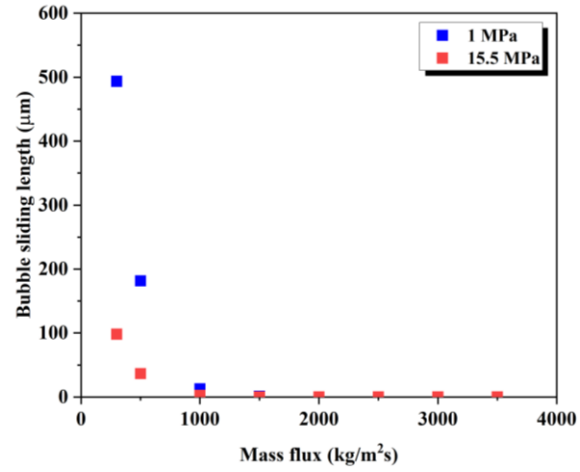

(b)

Figure 2. Calculated bubble departure and lift-off diameter (a), and sliding length (b) as a function of mass flux

3.1.3. Entrance length

The flow boiling aspects vary with flow regimes [12]. The coolant in APR1400 is fully developed before it is heated with fuel rods that the velocity profile is uniform along the fuel direction. Therefore, the entrance length of the test section was calculated with Equation (17) to fulfill the corresponding flow condition. The entrance length for the fully developed flow can be calculated by

$$L = 1.359 D_h \mathrm{Re}_{D_h}^{0.25} \quad (17)$$

,where L, D_h, and Re_{D_h} each refer to entrance length, hydraulic diameter, and Reynolds number for hydraulic diameter, respectively. The calculation was conducted under two pressure conditions (1 and 15.5 MPa) in the function of mass flux, and the results in Fig. 3 show that the maximum entrance length for the corresponding flow condition is approximately 120 mm.

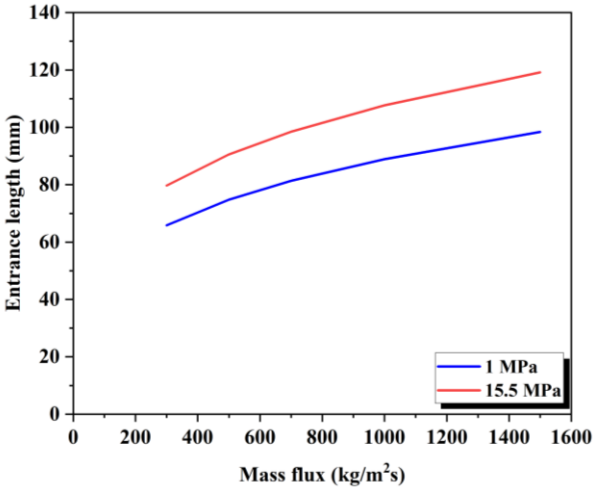

Figure 3. Calculated entrance length for fully developed flow in a function of mass flux

3.1.4. Working fluid temperature, pressure, and mass flux

The temperature and pressure of the working fluid were determined to be same as the subchannel conditions of APR1400 [13]. The system pressure of APR1400 is 15.5 MPa and the temperature varies from 290 to 320°C. Therefore, the apparatus was designed to be operated under corresponding conditions as shown in Table III.

Table III. Working fluid conditions of APR1400 and the experiment

Parameter	APR1400	Experiment
Pressure	15.5 MPa	1 ~ 15.5 MPa
Subcooling	20 ~ 30°C	20 ~ 40°C
Temperature	290 ~ 320°C	140 ~ 320°C
Mass flux	3600 kg/m^{2}s	500 ~ 1500 kg/m^{2}s

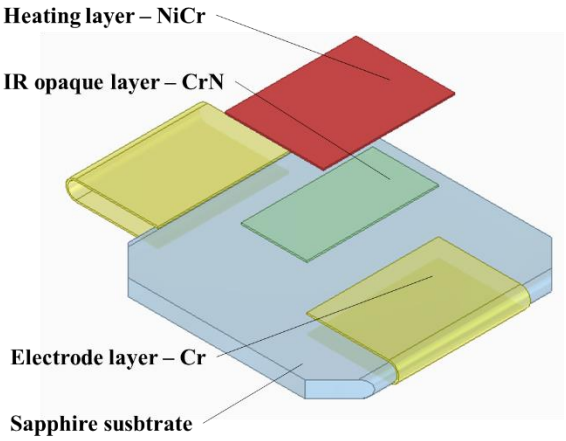

Figure 4. Test sample

3.2. Test Sample

The test sample is designed by depositing CrN, Cr, and NiCr layers on a sapphire substrate as shown in Fig. 4. The sapphire substrate has a flat area of 15 × 15 mm^2 and a thickness of 1 mm. Two sides of its thickness are in a round shape that the Cr layer deposited on the top and the bottom face could be connected through. The CrN layer works as a temperature measurement layer as CrN is opaque to infrared rays. NiCr lies over the CrN layer with a thickness of 100 nm to work as a heating layer and bubbles will be nucleated on the corresponding layer. The NiCr layer will be heated by Joule's heating and two Cr electrode layers exist at each side of the heating layer. NiCr will be heated when electrical power is applied to the Cr layer as Cr has low specific resistance compared to NiCr.

3.3 Test section

The test section is composed of the heater cartridge, window cartridge, and main body. The heater cartridge is made of ceramic to hold the test sample in the middle and avoid the leakage of current as shown in Fig. 5. The sample is pressed by two stainless clamps. Two copper electrodes are connected to the sample from the bottom and supply electrical power from the external source. Two holders are inserted into the cartridge body so that it could be connected to the main body. The window cartridge is also made of ceramic and it holds a sapphire window and makes a flow channel.

The main body is made of stainless steel to be operated under high pressure and temperature conditions as shown in Fig. 6. A rectangular flow channel penetrates through the middle of the body. The heater and the window cartridges are connected to the body and two spaces for nitrogen gas and water exist. When the water at high pressure flows through the channel, the nitrogen gas at the same pressure exists on the opposite side of the sample for a pressure balance. This balance prevents the sample to be broken during the experiment. On the opposite side of the window cartridge, the water with the same pressure as the working fluid is filled to prevent the sapphire window from breaking.

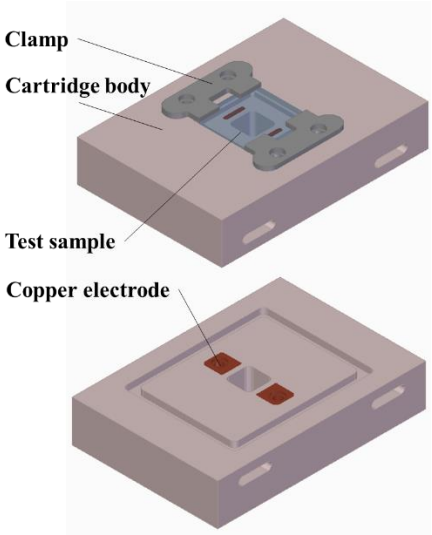

Figure 5. Heater cartridge

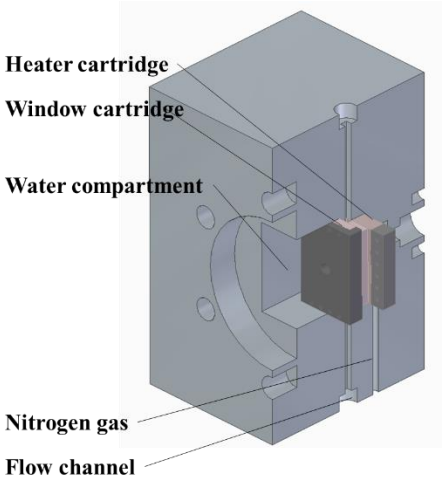

Figure 6. Main body

Two sapphire windows are inserted into the main body at the bottom and the top surfaces. The window at the bottom of the sample surface allows an IR measurement of boiling heat transfer to visualize wall temperature and heat flux distribution. Through the top window, bubble nucleation in and its dynamics such as departure from the site and sliding can be visualized using a high-speed video camera.

3.4. Flow loop

A schematic diagram of the flow loop is shown in Fig. 7 that it is divided into three loops: pressurizing loop, test loop, and nitrogen gas loop. The pressurizing loop is designed to develop pressure and temperature conditions of the working fluid. The fluid is pressurized through the pressurizing pump (1) at the maximum flow rate of 0.6 lpm. The pressure is controlled by the regulator (2). The pressurized fluid is primarily heated by the heater (3) and moves into the agitator tank (4).

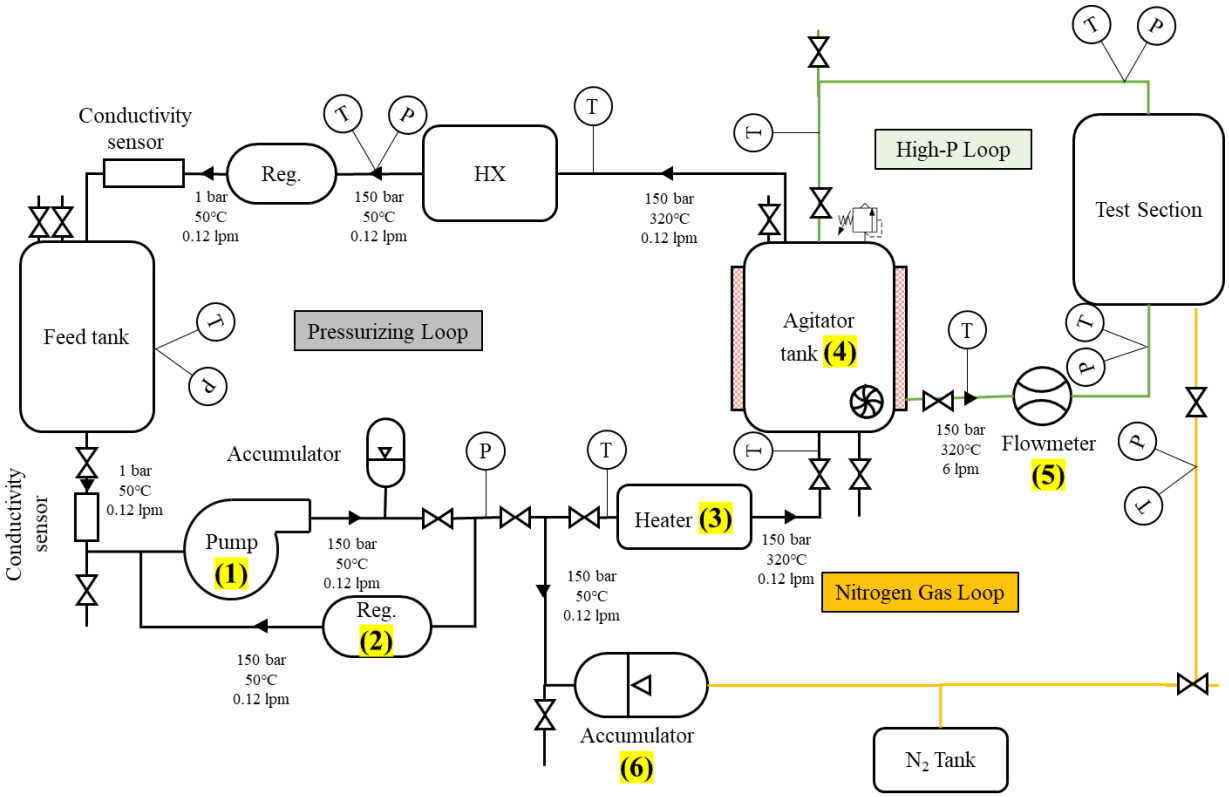

Figure 7. Flow loop

The flow loop is designed to flow the pressurized and heated fluid into the test section with a relatively high velocity compared to the pressurizing loop. An agitator inside the tank (4) generates a mass flux of the fluid to be up to 3500 kg/m^{2}s. The velocity is detected by the Coriolis mass flow meter (5) before moving into the test section.

The nitrogen gas loop is designed to supply the gas into the test section, maintaining the same pressure as the working fluid. The loop is connected with the pressurizing loop through an accumulator (6) so that the pressure of the gas and the fluid are continuously kept the same.

4. Conclusion

As bubble dynamics parameters play an important role in predicting boiling heat transfer, CFD includes corresponding models. However, the models used in CFD are only validated at high-pressure pool boiling or intermediate-pressure flow boiling experiments. To improve the preceding models, it is necessary to obtain experimental bubble dynamics data at the high-pressure flow boiling condition. Therefore, an experimental apparatus including a test section and a flow loop was designed to be operated under the same hydraulic conditions as APR1400. High-precision data of the bubble dynamics including bubble departure diameter and nucleation site density will be measured using various advanced optical diagnostics to improve models used in CFD.

ACKNOWLEDGMENT

This work was supported by the National Research Foundation of Korea (NRF) grant funded by the Korea government (MSIT: Ministry of Science and ICT) (2019M2D2A1A02059364)

This work was supported by the Nuclear Safety Research Program through the Korea Foundation Of Nuclear Safety (KoFONS) using the financial resource granted by the Nuclear Safety and Security Commission (NSSC) of the Republic of Korea. (2106022)

REFERENCES

[1] N. Kurul and M.Z. Podowski, On the Modeling of Multidimensional Effects in Boiling Channels, ANS Proc. 27th National Heat Transfer Conference, Minneapolis, MN, 1991
[2] L. Gilman and E. Baglietto, A Self-Consistent, Physics-Based Boiling Heat Transfer Modeling Framework for Use in Computational Fluid Dynamics, Int. J. Multiphase Flow, Vol. 95, pp. 35-53, 2017
[3] G. Kocamustafaogullari and M. Ishii, Foundation of the Interfacial Area Transport Equation and Its Closure Relations, Int. J. Heat and Mass Transfer, Vol. 38, pp. 481-493, 1995
[4] V.I. Tolublinsky and D.M. Kostanchuk, Vapour Bubbles Growth Rate and Heat Transfer Intensity at Subcooled Water Boiling, Int. Heat Transfer Conference 4, Paris-Versailles, France, 1970
[5] H.C. Unal, Maximum Bubble Diameter, Maximum Bubble Growth Time and Bubble Growth Rate during Subcooled

Nucleate Flow Boiling of Water up to 17.7 MN/m^2, Int. J. Heat and Mass Transfer, Vol. 19, pp. 643-649, 1976
[6] R. Cole, A Photographic Study of Pool Boiling in the Region of the Critical Heat Flux, AlChe J., Vol. 6, pp. 533-542, 1960
[7] Q. Li et al., Development, Verification and Application of a New Model for Active Nucleation Site Density in Boiling System, Nucl. Eng. Design, Vol. 328, pp. 1-9, 2018
[8] T. Hibiki and M. Ishii, Active Nucleation Site Density in Boiling Systems, Int. J. Heat and Mass Transfer, Vol. 46, pp. 2587, 2006
[9] G. Kocamustafaogullari and M. Ishii, Interfacial Area and Nucleation Site Density in Boiling Systems, Int. J. Heat and Mass Transfer, Vol. 26, pp. 1377-1387, 1983
[10] P.A. Kew and K. Cornwell, Correlations for the Prediction of Boiling Heat Transfer in Small-Diameter Channels, Appl. Thermal Eng., Vol. 17, No. 8-10, pp. 705-715, 1997
[11] N. Basu et al., Wall Heat Flux Partitioning during Subcooled Flow Boiling: Part 1-Model Development, Int. J. of Heat Transfer, Vol. 127, pp. 131-140, 2005
[12] S.G. Kandlikar, Heat Transfer Characteristics in Partial Boiling, Fully Developed Boiling, and Significant Void Flow Regions of Subcooled Flow Boiling, J. Heat Transfer, Vol. 120, No. 2, pp. 395-401, 1998
[13] KEPCO and KHNP, Status Report 83 – Advanced Power Reactor 1400 MWe (APR1400), 2011